HHS Public Access

Author manuscript

J Control Release. Author manuscript; available in PMC 2022 September 10.

Published in final edited form as:

J Control Release. 2021 September 10; 337: 168–178. doi:10.1016/j.jconrel.2021.07.026.

Vaccine nanodiscs plus polyICLC elicit robust CD8+ T cell responses in mice and non-human primates.

Alireza Hassani Najafabadi[#1,2,3], **Zeynab Izadi Najaf Abadi**[#1,2], **Marisa E. Aikins**[#1,2], **Kathryn E. Foulds**[4], **Mitzi M. Donaldson**[4], **Wenmin Yuan**[1,2], **Emeka. B. Okeke**[1,2,5], **Jutaek Nam**[1,2,6], **Yao Xu**[1,2], **Priyan Weerappuli**[2], **Taryn Hetrick**[7], **David Adams**[8], **Patrick A. Lester**[7], **Andres M. Salazar**[9], **Dan H. Barouch**[10], **Anna Schwendeman**[1,2], **Robert A. Seder**[4], **James J. Moon**[1,2,11,*]

[1]Department of Pharmaceutical Sciences, University of Michigan, Ann Arbor, MI, 48109, USA.

[2]Biointerfaces Institute, University of Michigan, Ann Arbor, MI, 48109, USA.

[3]Department of Biomedical Engineering, University of Connecticut Health Center, Farmington, Connecticut 06030, USA

[4]The Vaccine Research Center, National Institute of Allergy and Infectious Diseases, National Institutes of Health, Bethesda, MD, 20892, USA.

[5]Department of Biology, State University of New York, Fredonia, NY, 14063, USA.

[6]College of Pharmacy, Chonnam National University, Gwangju 61186, Republic of Korea.

[7]Unit for Laboratory Animal Medicine, University of Michigan, Ann Arbor, MI, 48109, USA.

[8]Biomedical Research Core Facilities, University of Michigan, Ann Arbor, MI, 48109, USA.

[9]Oncovir, Inc., Washington, DC, 20008, USA.

[10]Center for Virology and Vaccine Research, Beth Israel Deaconess Medical Center, Harvard Medical School, Boston, MA 02215, USA.

[11]Department of Biomedical Engineering, University of Michigan, Ann Arbor, MI, 48109, USA.

[#] These authors contributed equally to this work.

Abstract

[*]Corresponding author. moonjj@med.umich.edu.

Credit Author Statement

AHN and JJM designed the experiments, interpreted the results, and wrote the manuscript. ZINA, MEA, MMD, WY, EBO, JN, and YX performed experiments. PW, TH, DA, and PAL contributed technical expertise. AMS provided polyICLC and DHB provided rAd vector. KEF, AS, and RAS aided with the design of experiments and interpretation of the results.

Disclosure of Potential of Conflicts of Interest

A patent application for nanodisc vaccines has been filed, with J.J.M., A.S., A.H.N., and J.N., as inventors. J.J.M. and A.S. are co-founders of EVOQ Therapeutics, LLC. that develops the nanodisc technology for vaccine applications. A.S. serves as the CEO and CSO of Oncovir that develops PolyICLC (Hiltonol®).

Conventional cancer vaccines based on soluble vaccines and traditional adjuvants have produced suboptimal therapeutic efficacy in clinical trials. Thus, there is an urgent need for vaccine technologies that can generate potent T cell responses with strong anti-tumor efficacy. We have previously reported the development of synthetic high-density protein (sHDL) nanodiscs for efficient lymph node (LN)-targeted co-delivery of antigen peptides and CpG oligonucleotides (a Toll-like receptor-9 agonist). Here, we performed a comparative study in mice and non-human primates (NHPs) to identify an ideal vaccine platform for induction of CD8+ T cell responses. In particular, we compare the efficacy of CpG class B, CpG class C, and polyICLC (a synthetic double-stranded RNA analog, a TLR-3 agonist), each formulated with antigen-carrying sHDL nanodiscs. Here, we report that sHDL-Ag admixed with polyICLC elicited robust Ag-specific CD8+ T cell responses in mice, and when used in combination with α-PD-1 immune checkpoint inhibitor, sHDL-Ag + polyICLC completely eliminated large established (~100 mm^3) MC-38 tumors in mice. Moreover, sHDL-Gag + polyICLC induced robust Simian immunodeficiency virus Gag-specific, polyfunctional CD8+ T cell responses in rhesus macaques and could further amplify the efficacy of recombinant adenovirus-based vaccine. Notably, while both sHDL-Ag-CpG-B and sHDL-Ag-CpG-C generated strong Ag-specific CD8+ T cell responses in mice, their results were mixed in NHPs. Overall, sHDL combined with polyICLC offers a strong platform to induce CD8+ T cells for vaccine applications.

GraphicalAbstract

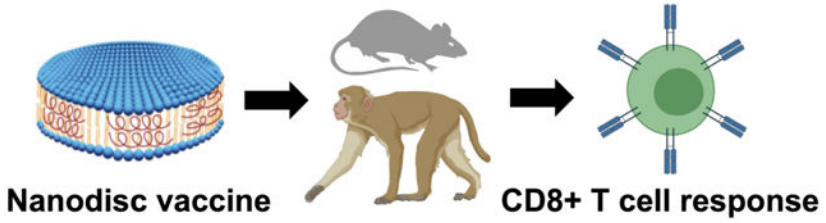

1. Introduction.

Cancer immunotherapy based on vaccinations aims to elicit CD8+ T cell responses against tumor antigen (Ags). However, conventional vaccine strategies based on soluble vaccine formulations have produced suboptimal anti-tumor effects in clinical trials. This limitation has been attributed in part to the inefficient delivery of Ags to the sites of immune activation, such as lymph nodes (LNs), as well as poor immunogenicity of Ags [1, 2]. Thus, strong immunostimulatory agents are required to induce the maturation of antigen-presenting cells (APCs) and CD8+ cytotoxic T lymphocyte responses. Various approaches have been introduced to increase the efficacy of adjuvant systems, including lipid-conjugated adjuvants [3], encapsulation of adjuvants within nanoparticle carriers [4], and stabilization of adjuvants with polymers to form immunostimulatory nanoparticles (for example, Hiltonol [5]). While these are encouraging, it still remains unknown how the efficacy of various adjuvants compare, especially when used in the context of LN-targeted nanoparticles designed for cancer immunotherapy. Here, we aimed to address these issues by performing a comparative study using Ag-loaded nanoparticles formulated with synthetic nucleic acid-based adjuvants, including CpG DNA oligonucleotides (ODNs) and polyinosine-polycytidylic acid (polyIC,

a synthetic double-stranded RNA analog). Of note, these adjuvants all induce Type 1 IFN which is required for efficient cross-priming of CD8+ T cells with non-live vaccine platforms. Here, we report our analysis of CD8+ T cell responses in mice and non-human primates (NHPs) vaccinated with nanoparticleadjuvant formulations. Notably, NHPs have a similar cellular distribution of TLRs as humans [6], thus providing data that may be more translatable.

CpG ODNs are a potent Toll-like receptor (TLR)-9 agonist that has been studied in various cancer vaccine clinical trials [7, 8]. Based on the structure and immunostimulatory activity, CpG is classified into three classes. CpG class A ODNs are comprised of two poly-G tail regions with phosphorothioate backbones linked by a double-stranded – hairpin-like – region containing a palindromic CpG-motif with a phosphodiester backbone region. CpG-A ODNs are potent stimulators of IFN-α production from plasmacytoid dendritic cells (pDCs) but weak inducers of TLR-9 dependent pro-inflammatory cytokine production [9]. CpG class B ODNs are comprised of CpG dinucleotides with a phosphorothioated backbone. CpG-B ODNs are potent activators of B-cells, pDCs, and monocytes, but they are relatively weak stimulators of IFN-α production [10]. Lastly, CpG class C, a hybrid of CpG-A and CpG-B ODNs [11], is composed of a palindromic CpG-motif region and a phosphorothioated backbone. CpG-C ODNs are potent stimulators of IFN-α production from pDCs and activators of B-cells [12-15].

Another potent adjuvant is polyIC, a synthetic double-stranded RNA analog. PolyIC, like viral double-stranded RNA, can activate DCs, macrophages, and stromal cells via TLR-3 and melanoma differentiation-associated protein-5 (MDA5) [16, 17]. PolyIC induces IL-12 and type-I IFN secretion and activates cytosolic receptors, such as retinoic acid-inducible gene-1(RIG-I) and MDA-5 [17, 18]. However, naked polyIC is rapidly broken down *in vivo* by serum and tissue ribonucleases. To avoid this issue, polyIC is stabilized with poly-L-lysine and carboxymethylcellulose to form nanoparticles, termed polyICLC (also known as Hiltonol®) [19]. PolyICLC is resistant to ribonucleases and induces potent type-I IFN secretion and T cell immune responses in mice, NHPs, and humans [19, 20]. PolyICLC is currently evaluated in various clinical trials [19].

We have previously reported the development of synthetic high-density protein (sHDL) nanodiscs for the co-delivery of peptide Ags and cholesterol-3’ end-modified CpG-B [21, 22]. The small size of sHDL (10 nm), well-documented safety profiles, and its unique ability to target Ags and adjuvants to DCs residing in LNs after subcutaneous administration make sHDL a promising vaccine delivery system. Nevertheless, our previous studies on sHDL nanodiscs have mainly focused on the delivery of Ags and CpG-B [23]; however, CpG-C also has been reported to offer strong immune activation in mice and NHPs [24, 25]. In addition, since we have so far used only CpG-B tethered with cholesterol tail at 3’ end of CpG ODN, here, we sought to compare the efficacy of sHDL vaccine delivering CpG-B or CpG-C, each modified with cholesterol tail at either 3’ or 5’ end of CpG. Furthermore, we examined sHDL vaccine coformulated with polyICLC. As polyICLC is already in a nanoparticle form with an average diameter of 100 nm, we simply admixed Ag-loaded sHDL with polyICLC. Using both CpG and polyICLC, we sought to identify an ideal adjuvant to use with nanodiscs (either admixed or codelivered) for future clinical translation.

Here, we have compared the efficacy of CpG-B, CpG-C, and polyICLC, each formulated with antigen-carrying sHDL nanodiscs. We have examined their effects on induction of Ag-specific CD8+ T cell responses in mice and studied their anti-tumor efficacy when used in combination with α-PD-1 immune checkpoint inhibitor in MC-38 tumor-bearing mice. Moreover, we sought to explore the efficacy of antigen-carrying sHDL nanodiscs formulated with CpG-B, CpG-C, or polyICLC in terms of eliciting Ag-specific polyfunctional CD8+ T cell responses in rhesus macaques. Briefly, we report that both sHDL-Ag-CpG-B and sHDL-Ag-CpG-C generated strong Ag-specific CD8+ T cell responses in mice, whereas sHDL-Ag-CpG-B elicited higher CD8+ T cell response than sHDL-Ag-CpG-C in rhesus macaques. We also show that sHDL-Ag admixed with polyICLC significantly improved Ag-specific CD8+ T cell responses both in mice and rhesus macaques. We also report that vaccine nanodisc could serve as a prime vaccine for a boost with recombinant adenovirus-based vaccine. Taken together, the sHDL system provides a strong platform for vaccine applications.

2. Experimental section.

2.1. Materials and methods.

Adpgk (CSSASMTNMELM) neoantigen and CM9 (CTPYDINQM) peptides were synthesized by RS Synthesis (Louisville, KY). 22A Apolipoprotein-A1 mimetic peptide was synthesized by GenScript (Piscataway, NJ). Antibody against mouse PD-1 was purchased from BioXCell (West Lebanon, NH). 1,2-dimyristoyl-sn-glycerol-3-phosphocholine (DMPC) was purchased from NOF America (White Plains, NY). 1,2-dioleoyl-sn-glycero-3-phosphoethanolamine-N-[3-(2-pyridyldithio)propionate] (DOPE-PDP) was purchased from Avanti Polar Lipids (Alabaster, AL). CpG-1826 (Class B CpG: 5′-tccatgacgttcctgacgtt-3′), CpG-2395 (Class C CpG: 5′-tcgtcgttttcggcgcgcgccg-3′), and CpG-7909 (Class B CpG: 5’-tcgtcgttttgtcgttttgtcgtt-3’) (lower case letters indicate phosphorothioate linkage) with or without cholesterol tag were synthesized by Integrated DNA Technologies (Coralville, IA). Hiltonol® (polyICLC) was kindly provided by Dr. Andres Salazar (Oncovir Inc., Washington DC, USA). Cell media was purchased from Invitrogen (Carlsbad, CA).

2.2. Synthesis and characterization of Adpgk incorporated sHDL nanodiscs.

Lipid-peptides were prepared as previously reported [22]. To incorporate Adpgk neoantigen peptides or CM9 into sHDL nanodiscs, peptides were modified with a cysteine at the N-terminus. Cysteine-displaying peptides were reacted with DOPE-PDP (Ag peptide/DOPE-PDP = 2:1, molar ratio) for 4 hr on an orbital shaker in dimethylformamide (DMF). The conjugation efficiency of the reaction was calculated based on the reduction in the absorbance signal associated with DOPE-PDP as measured by reverse-phase high-performance liquid chromatography (HPLC), as we reported previously [22, 26, 27]. sHDL was prepared as previously described [22, 28]. Briefly, sHDL were synthesized by dissolving 22A Apo-A1 peptide and DMPC in acetic acid, evaporating acetic acid by freeze dryer to form a desiccated lipid film, and rehydrating this film with 10 mM sodium phosphate buffer. Incorporation of prepared lipid-peptide complex into sHDL to make sHDL-Ag was achieved by dissolving lipid-peptide complexes in DMSO and titrating the mixture into sHDL suspension. The mixture was incubated for 1 hr at room temperature

on an orbital shaker at 200 rpm to incorporate lipid-peptides into sHDL nanodiscs. Unincorporated lipid-peptide conjugates were then separated by ultracentrifuge-driven filtration (MilliporeSigma™ Amicon™ Ultra Centrifugal Filter, 10KD). Reverse-phase HPLC was used to measure the efficiency of lipid-peptide conjugation and incorporation, as we reported previously [22, 26, 27]. To prepare sHDL-Ag + polyICLC, sHDL-Ag was simply admixed with polyICLC before immunization. To load CpG into sHDL-Ag, aqueous solutions of cholesterol-modified (3' or 5')-CpG ODNs 1826, 2395, or 7909 (Integrated DNA Technologies) were titrated into sHDL-Ag at a DMPC to CpG weight ratio of 50:1 and incubated at room temperature with gentle shaking on an orbital shaker for 1 hr. ODN loading was quantified by gel permeation chromatography (GPC) equipped with TSKgel G3000SWxl column (7.8 mm ID × 30 cm, Tosoh Bioscience LLC). The hydrodynamic sizes and zeta potentials of nanodisc samples were measured by dynamic light scattering (DLS, Zetasizer Nano ZSP). The morphology of sHDL nanodiscs was visualized by transmission electron microscopy after fixation via osmium tetroxide. TEM images were obtained by a JEM 1200EX electron microscope (JEOL USA) equipped with an AMT XR-60 digital camera (Advanced Microscopy Techniques).

2.3. Activation of bone marrow-derived dendritic cells.

Bone marrow-derived dendritic cells (BMDCs) were generated as previously described [3]. Briefly, bone marrow was flushed from femur and tibia bones of 5 to 6 weeks old C57BL/6 mice. Isolated bone marrow cells were plated at 1×10^6 cells per dish in RPMI 1640 supplemented with 10% FBS, 55 μM β-mercaptoethanol, 20 ng/ml of GM-CSF, and 100 U/ml penicillin. On days 3 and 5, half of the culture media was replaced with fresh media. On day 8, BMDCs were harvested and plated at 1×10^6 cells per well in 12-well plates. After 24 hrs, BMDCs incubated with 23 nM CpG (3'or 5'-CpG type B or C) or 20 μg of polyICLC for 24 hrs at 37 °C with 5% CO_2. Supernatants were then collected, and the levels of different inflammatory cytokines were measured by ELISA (Enzyme-linked immunosorbent assay). BMDCs were then washed twice with FACS buffer (1% BSA in PBS), incubated with anti-CD16/32 at room temperature, and then stained on ice with fluorophore-labeled antibodies against CD11c, CD40, CD80, and CD86. Cells were then washed twice by FACS buffer, resuspended in 2 μg/mL DAPI solution, and analyzed by flow cytometry.

2.4. Immunization studies in mice.

Mice were cared for following the federal, state, and local guidelines. University of Michigan, Ann Arbor is an AAALAC International accredited institution, and all work conducted on mice was approved by the University of Michigan Institutional Animal Care and Use Committee (IACUC). Female C57BL/6 mice (5–6 weeks) were purchased from Jackson Laboratory (Bar Harbor, ME). C57BL/6 mice were immunized subcutaneously at the tail base on days 0, 14, and 28. Each vaccine dose contained 15.5 nmol of Adpgk peptide and 2.3 nmol of CpG or 60 μg of polyICLC in either soluble or sHDL forms. Seven days after each immunization, peripheral blood mononuclear cells (PBMCs) were collected via submandibular bleeding. Red blood cells were lysed with Ammonium-Chloride-Potassium (ACK) lysis buffer. Tetramer staining assays were performed to quantify the percentage of tumor Ag-specific CD8a+ T cells among PBMCs, as described previously [29, 30].

PBMCs were isolated, washed with FACS buffer, and incubated with anti-CD16/32 blocking antibody. Cells were incubated with tetramer for 1 hr on ice and then with anti-mouse CD8a-APC for 20 min on ice. Cells were washed twice with FACS buffer, resuspended in DAPI solution (2 μg/ml), and analyzed by flow cytometry.

For therapeutic studies in MC-38 tumor-bearing animals, C57BL/6 mice were inoculated subcutaneously with 1×10^6 MC-38 cells in the right flank on day 0. Tumor-bearing animals were then immunized subcutaneously at the tail base on day 6 or 10, followed by a booster vaccination after 7 days – a dosing schedule that is in line with our prior studies [26, 27]. Each vaccine dose was 15.5 nmol of Adpgk peptide and 2.3 nmol of CpG or 60 μg of polyICLC in either soluble or sHDL form. In a subset of studies, anti-mouse αPD-1 antibody (100 μg per mouse) was administered intraperitoneally on days 1 and 4 after each vaccination. Tumor growth was observed every other day, and the tumor volume was reported using the following equation: tumor volume = length × $(\text{width})^2 \times 0.5$. Animals were euthanized when the tumor mass reached 1.5 cm in any dimension or when animals became moribund with > 20% weight loss or ulceration.

2.5. Immunization studies in non-human primates

Mamu-A*01 rhesus macaques (*Macaca mulatta*) used in these studies (males and females, 3-8 years old) were purchased from Johns Hopkins University and Primgen. Macaques were stratified into comparable groups based on age, weight, and sex. All experimentation complied with federal, state, and local regulations and ethical guidelines at the respective institutions (Animal Care and Use Committees of the Vaccine Research Center, NIAID, NIH, Bioqual, Inc., and University of Michigan). Macaques were housed and cared for in Bioqual in accordance with local, state, federal, and institute policies in facilities accredited by the AAALAC International, under standards established in the Animal Welfare Act and the Guide for the Care and Use of Laboratory Animals, 8th ed. Macaques were monitored for physical health, food consumption, body weight, temperature, complete blood counts, and serum chemistries. Macaques (n = 3/group) were immunized on weeks 0, 4, 8, and 12 with the sHDL nanodisc formulations. The dosing schedule was in line with prior subunit vaccine studies in NHPs [31-33]. CM9 peptide was dosed at 400 μg on each time point. Adjuvants included 1 mg Hiltonol, 60 nmol cholesterol-CpG-7909 (CpG-B), or 60 nmol cholesterol-CpG-2395 (CpG-C) on each time point. The vaccine doses were chosen based on prior reports on NHP vaccination [25, 34]. Each vaccine dose was divided into four and administered subcutaneously (500 μl injection volume per site): subcutaneous L and R behind the knee and subcutaneous L and R inner thigh. On week 24, all animals were boosted with 10^{10} virus particles of replication-defective recombinant SIVmac239-Gag Ad5 vector by intramuscular vaccination at the left and right quadriceps (500 μL volume each, 1 mL total injection volume). In addition, three animals received SIVmac239-Gag Ad5 vector only without primary immunization.

Bronchoalveolar lavage fluid (BAL) was collected on weeks −1, 8, 16, 24, 26, and 28. BAL cells were stimulated in R-10 medium (RPMI 1640 supplemented with 10% FCS, 2 mM Lglutamine, 25 mM HEPES, and penicillin–streptomycin) in the presence of brefeldin A (10 μg/ml) with or without SIV Gag CM9 peptide (2 μg/ml). After stimulation at 37°C

in 5% CO2 for 6 h, cells were stained as described previously [35]. Cells were washed, fixed, permeabilized, and stained for CD3, CD4, CD8, CD28, CD45RA, CCR7, CD69, IFN-γ, TNF-α, and IL-2 for 20 min at room temperature in the dark. Cells were acquired with FACSymphony (BD Biosciences) and DiVa software. Post-acquisition analyses were performed with FlowJo software. Data shown on the graphs represent values of SIV Gag CM9 peptide stimulated cells from which background values (no peptides) have been subtracted.

2.6. Statistical analysis.

Sample sizes were selected according to pilot experiments and previous literature. Data were analyzed by one-way or two-way ANOVA, followed by Tukey's multiple comparisons posttest or log-rank (Mantel-Cox) test with Prism 8.0 (GraphPad Software). Statistical significance is indicated as *P < 0.05, **P < 0.01, ***P < 0.001 and ****p < 0.0001. All values are reported as mean ± SEM, showing a representative experiment from 2-3 independent experiments.

3. Results and discussion.

3.1. Synthesis and characterization of sHDL nanodiscs.

Nanodiscs were generated by mixing 1,2-dimyristoyl-sn-glycerol-3-phosphocholine (DMPC) and 22A apolipoprotein-A1 mimetic peptide, followed by lyophilization, reconstitution in 10 mM phosphate buffers, and heating/cooling cycles to form sHDL. Afterwards, cysteine pre-modified Ag peptides (i.e. Adpgk and CM9 peptides) were reacted with 1,2-dioleoyl-sn-glycero-3-phosphoethanolamine-N-[3-(2-pyridyldithio)propionate] (DOPE-PDP) in DMF. Next, peptide-lipid conjugates in DMSO were added dropwise to sHDL. Using HPLC, we quantified the amount of peptides conjugated to DOPE-PDP and subsequently incorporated into nanodiscs (Figure 1A,B). HPLC chromatograms showed the disappearance of DOPE-PDP peak (23 min) and appearance of new peak attributed to the lipid-peptide conjugates (22 min), indicating successful conjugation of cysteine-modified peptides. Overall, the HPLC analyses showed successful synthesis of DOPE-peptide with > 90% conjugation efficiency. Additionally, sHDL nanodiscs were efficiently loaded with lipid-peptide conjugates with 90 ± 8% and 90 ± 5% loading efficiency for Adpgk and CM9 Ag peptide, respectively.

Next, cholesterol-modified CpG (cho-CpG) was mixed and incubated with sHDL-Ag nanodiscs at a DMPC:cho-CpG weight ratio of 50:1. For our murine studies, we employed CpG-1826 (CpG-B) and CpG-2395 (CpG-C), each with cholesterol tethered at either 3' or 5' terminus of CpG ODN. The resulting Ag/CpG-loaded sHDL nanodiscs (sHDL-Ag-CpG) were analyzed by DLS. All nanodisc samples exhibited average diameters of 10-12 nm with no significant variability observed between CpG-B and CpG-C subtypes (Figure 2A and Table 1). TEM images showed that sHDL-Adpgk-3'-CpG-C had uniform size and nanodisc-like morphology with an average diameter of 10 ± 3 nm (Figure 2B), which was consistent with the DLS results. GPC analyses indicated that cho-CpG was consistently loaded into sHDL-Adpgk nanodiscs with ~90% loading efficiency, regardless of CpG-B and

CpG-C subtypes or the site of cholesterol conjugation at either 3’ or 5’ terminus of CpG ODN (Figure 2C-F, and Table 1).

3.2. Activation of bone marrow-derived dendritic cells (BMDCs).

Next, we evaluated immunostimulatory properties of sHDL formulated with either polyICLC, CpG-B, or CpG-C. Since polyICLC is already in a particulate form with an average diameter of 100 nm, we simply admixed polyICLC with sHDL. For CpG-B and CpG-C, sHDL nanodiscs were loaded as above with either CpG-B or CpG-C containing cholesterol tail conjugated at 3’ or 5’ terminus of ODN. We examined their immunostimulatory activities by incubating them with BMDCs for 24 hr *in vitro*, followed by measuring the expression levels of co-stimulatory ligands, including CD40, CD80, and CD86, and quantifying cytokines, including IL-12p70, IL-6, and TNF-α. For the control groups, we employed free soluble CpG-B and CpG-C without cholesterol in the presence or absence of blank sHDL. Without the cholesterol tail, CpG was not incorporated into blank sHDL (data not shown). In addition, sHDL admixed with free polyIC was included as a control for the sHDL + polyICLC group.

Our results showed that sHDL + polyICLC, sHDL-3’-CpG-B, and sHDL-3’-CpG-C significantly up-regulated the expression levels of CD40, CD80, and CD86 on BMDCs ($P < 0.0001$, Figure 3A-C), compared with their respective free adjuvant controls as well as sHDL-5’-CpG-B and sHDL-5’-CpG-C. Similarly, BMDCs incubated with sHDL + polyICLC, sHDL-3’-CpG-B, or sHDL-3’-CpG-C significantly increased the secretion of IL-12p70, IL-6, and TNF-α ($P < 0.0001$, Figure 3D-F), compared with BMDCs treated with their respective free adjuvant controls as well as sHDL-5’-CpG-B and sHDL-5’-CpG-C. Overall, these results showed that sHDL + polyICLC promoted more robust DC activation than sHDL + polyIC. Moreover, these results indicated that sHDL-mediated delivery of CpG increased its potency and that 3’ end-modified CpG was more potent than 5’ end-modified CpG. This observation is in line with previous reports suggesting the crucial role of 5’ terminus of CpG-ODN in immune activation and engagement with TLR-9 [24, 36]. Based on these results, we focused our subsequent *in vivo* studies on sHDL + polyICLC, sHDL-3’-CpG-B, and sHDL-3’-CpG-C. For simplicity, sHDL-3’-CpG-B, and sHDL-3’-CpG-C are henceforth termed as sHDL-CpG-B, and sHDL-CpG-C.

3.3. Nanodiscs elicit strong CD8+ T cell responses in mice.

We next studied CD8+ T cell responses generated by these sHDL vaccine formulations. Naíve C57BL/6 mice were immunized on days 0, 14, and 28 with 2.3 nmol CpG or 60 μg of polyICLC (Figure 4A). As a model Ag, we included a fixed dose of 15.5 nmol Adpgk peptide, which is a neoantigen previously identified in MC-38 colon carcinoma [37]. We analyzed vaccinated mice on day 7 after each immunization for the frequency of Adpgk-specific CD8+ T cells among PBMCs using the tetramer staining assay (Figure 4B,C). On day 7, mice immunized with all three sHDL formulations (i.e., sHDL-Ag + polyICLC, sHDL-Ag-CpG-C, and sHDL-Ag-CpG-B) elicited robust frequencies of Adpgk-tetramer+ CD8+ T cells (Figure 4B). Boost immunizations further amplified Adpgk-specific CD8+ T cell responses by day 35, achieving 7-fold, 5-fold, and 11-fold increases for sHDL-Ag + polyICLC, sHDL-Ag-CpG-C, and sHDL-Ag-CpG-B, compared with their respective soluble

vaccine controls ($P < 0.0001$, Figure 4B-C). Notably, all three sHDL vaccine formulations generated robust and comparable CD8+ T cell responses, except for a statistically significant higher T cell response for sHDL-Ag + polyICLC on day 21, compared with sHDL-Ag-CpG-B ($P < 0.05$, Figure 4B).

3.4. Nanodiscs exerts strong anti-tumor efficacy in mice.

Having shown that sHDL + polyICLC and sHDL-CpG-C induced potent cellular immune responses, we next examined their anti-tumor efficacy in a therapeutic setting (Figure 5). C57BL/6 mice were inoculated subcutaneously in their flank with $1x10^6$ MC-38 colon cancer cells. On day 6, when tumors were established with an average tumor volume of 70 mm^3, mice were immunized subcutaneously at the tail base with soluble or sHDL formulations of 15.5 nmol Adpgk neoantigen peptide with either 2.3 nmol CpG or 60 μg polyICLC (Figure 5A). On days 13 and 20, booster immunizations were administered. We performed tetramer staining assay on days 11 and 18 and quantified the percentage of Ag-specific CD8+ T cells among PBMCs (Figure 5B). Both sHDL + polyICLC and sHDL-CpG-C formulations elicited robust Ag-specific CD8+ T cells by day 11 (Figure 5B). In particular, sHDL-CpG-C induced 17.5% Ag-specific CD8+ T cell responses by day 18, representing a 2.5-fold increase, compared with Adpgk admixed with free CpG-C ($P < 0.05$, Figure 5B). Notably, sHDL-Ag + polyICLC exhibited more robust tumor control at the earlier time points, compared with sHDL-Ag-CpG-C ($P < 0.05$, Figure 5C). Nevertheless, both sHDL-Ag + polyICLC as well as sHDL-Ag-CpG-C formulations exerted robust anti-tumor efficacy against established tumors (Figure 5C), leading to tumor eradication in 3 out of 7 animals (Figure 5D). All the other soluble vaccine controls as well as sHDL-Ag-CpG-B exhibited only modest anti-tumor effects, with only 1 out of 7 animals tumor free by day 75 (Figure 5D).

It was notable that in our prior study reporting the development of sHDL vaccine [22], we employed a reduced number of 10^5 MC-38 tumor cells and demonstrated the anti-tumor effects of sHDL-Adpgk-CpG-B. In this current study, to differentiate the effects of adjuvants, we pressure-tested our system with 10-fold higher number of MC-38 tumor cells, and the results indicated that sHDL-Adpgk-CpG-C and sHDL-Adpgk + polyICLC resulted in higher rate of complete responders, compared with sHDL-Adpgk-CpG-B.

We next examined the therapeutic efficacy of sHDL vaccination combined with α-PD-1 IgG immunotherapy against large tumors (~100 mm^3) (Figure 6A). C57BL/6 mice were inoculated subcutaneously with $1x10^6$ MC-38 colon cancer cells in their flank. On day 10, when tumors were established an average tumor volume of 100 mm^3, mice were immunized subcutaneously at the tail base with soluble or sHDL formulations of 15.5 nmol Adpgk neoantigen peptide with either 2.3 nmol CpG or 60 μg polyICLC (Figure 6A). On day 17, a booster immunization was administered. Mice also received intraperitoneral administration of 100 μg α-PD-1 IgG on days 11, 14, 18, and 21. ELISPOT assay performed on splenocytes on day 35 indicated that sHDL-Ag + polyICLC combined with α-PD-1 IgG elicited more potent Adpgk neoantigen-specific IFN-γ+ T cell responses, compared with Ag + polyICLC ($P < 0.001$) as well as sHDL-Ag-CpG-B ($P < 0.01$), each combined with α-PD-1 IgG therapy (Figure 6B,C). Also, sHDL-Ag-CpG-C + α-PD-1 generated stronger

neoantigen-specific IFN-γ+ T cell responses, compared with sHDL-Ag-CpG-B + α-PD-1 ($P < 0.001$, Figure 6B,C).

Strikingly, sHDL-Ag + polyICLC combined with α-PD-1 regressed established tumors in 100% of animals, achieving significantly enhanced anti-tumor efficacy ($P < 0.05$, Figure 6D), compared with Ag + polyICLC combined with α-PD-1 therapy that had only ~29% complete response rate (Figure 6E). There was no sign of tumor recurrence for 100 days for all mice in the sHDL-Ag + polyICLC + α-PD-1 group (Figure 6F). In addition, sHDL-Ag-CpG-C + α-PD-1 therapy exerted robust anti-tumor efficacy and eradicated tumors in ~70% of animals (Figure 6D-F), whereas sHDL-Ag-CpG-C + α-PD-1 therapy exhibited ~43% response rate. Overall, these results indicated that sHDL-Ag + polyICLC vaccine in combination with α-PD-1 therapy exerted robust anti-tumor efficacy against large tumors. Unfortunately, due to the large number of comparison groups, there was no statistical difference for different sHDL adjuvant systems in terms of animal survival. However, there was a clear trend for increased complete responders and animal survival with the following order: sHDL-Ag + polyICLC + α-PD-1 > sHDL-Ag-CpG-C + α-PD-1 > sHDL-Ag-CpG-B + α-PD-1.

3.5. Nanodiscs elicit robust T cell responses in non-human primates (NHPs).

Encouraged by the results presented above, we sought to translate our results and evaluate the immunogenicity of sHDL vaccine nanodiscs in rhesus macaques. Because there is no tumor antigen reported in rhesus macaques, instead we employed CM9 Ag peptide, a SIVmac239 Gag immunodominant, MHC-I-restricted epitope in *Mamu*-A*01 rhesus macaques [34, 38, 39]. Notably, immunogenicity of polyICLC has been well documented in mice, NHPs, and humans [19, 40], while CpG-2395 (CpC-C) used in our studies above have been shown to elicit immune resposes in mice and NHPs [24, 25]. Hence, in our NHP studies, we used the same adjuvants from above to formulate sHDL-CM9 + polyICLC and sHDL-CM9-CpG-C vaccines. In contrast, CpG-1826 (CpG-B) used in our murine studies has not been previously tested in NHPs. Therefore, in our NHP studies, we formulated sHDL-CM9-CpG-B using CpG-7909 (CpG-B type), which has been tested and shown to generate immune responses in NHPs and humans [41-44].

We examined CM9-specific memory CD8+ T cells in BAL in *Mamu*-A*01 rhesus macaques over the course of sHDL vaccination (Figure 7A). One week prior to the prime vaccination, we confirmed that animals had a minimal level of Ag-specific CD8+ T cells (Supplementary Figure 1). Immunizations with sHDL-Ag + polyICLC produced robust Gag CM9-specific, polyfunctional (IFN-γ+/IL2+/TNF-α+) memory CD8+ T cell responses, achieving ~1.2% CM9-specific CD8+ T cells in BAL tissues on week 16 after 4 immunizations (Figure 7B). On the other hand, NHPs immunized with sHDL-Ag-CpG-C or sHDL-Ag-CpG-B generated detectable but weaker CM9-specific T cell responses (Figure 7C) although the differences were not statistically significant.

Next, after the 4^{th} sHDL vaccination, we rested immunized NHPs for 10 weeks and then administered a boost immunization with 10^{10} virus particles of replication-defective recombinant Ad5 vector encoding SIVmac239-Gag (rAd) (Figure 7A). Naíve NHPs that received rAd vaccine alone (without sHDL priming) served as a control group. Here, we

sought to examine whether sHDL vaccine could be “combined” with other conventional vaccines in the setting of heterologous prime-boost regimen. Notably, Ad5 vector is currently examined in various SARS-CoV-2 vaccines. The Sputnik V, licensed for the emergency use in Russia has Ad26 and Ad5-vectored formulations, while a single dose of Ad5-vectored COVID19 vaccine is approved for emergency use in China, Mexico, and Pakistan [45]. However, due to concerns of anti-vector immunity with homologous vaccination [46], rAd vector-based vaccinations require changes in the capsid design for each vaccination.

After 10 weeks of resting, sHDL-immunized NHPs exhibited low but detectable levels of CM9-specific memory CD8+ T cells in BAL (Supplementary Figure 1). After the rAd boost immunization, NHPs previously immunized with sHDL-Ag + polyICLC further expanded polyfunctional (IFN-γ+/IL2+/TNF-α+) CD8+T cell responses, achieving 1.9% frequency of SIV Gag CM9-specific memory CD8+ T cells by week 28 (Figure 7C,D). Notably, this level of CD8+ T cell response was higher than that achieved in NHPs that just received rAd vaccination (without sHDL priming) (Figure 7C,D), suggesting the potential of sHDL + polyICLC as a platform for heterologous vaccination with viral vector-based vaccines. In addition, NHPs previously immunized with sHDL-Ag-CpG-B (CpG-7909) also expanded CM9-specific memory CD8+ T cells after the boost rAd vaccination (Figure 7C,D). In contrast, NHPs previously immunized with sHDL-Ag-CpG-C (CpG-2395) did not exhibit further expansion of CM9-specific CD8+ T cells after the boost rAd vaccination (Figure 7C,D). Taken together, these results suggest that sHDL + polyICLC is a potent vaccine system for induction of Ag-specific CD8+ T cell responses in NHPs. Notably, our earlier studies performed in MC-38 tumor-bearing mice (Figures 5, 6) indicated that both sHDL-Ag-CpG-B (CpG-1826) and sHDL-Ag-CpG-C (CpG-2395) elicited robust CD8+ T cell responses, and in particular, sHDL-Ag-CpG-C (CpG-2395) exerted strong anti-tumor efficacy against established MC-38 tumors. Yet, in NHPs, sHDL-Ag-CpG-B (CpG-7909) elicited higher CD8+ T cell response than sHDL-Ag-CpG-C (CpG-2395) although this difference was not statistically significant. This discrepancy between our mouse and NHP dataset may be attributed to the differences in the sequences of CpG type B (CpG-1826 vs. CpG-7909) used in our mouse versus NHP immunization studies as well as the differential expression of TLR9 among APCs in mice versus NHPs [43]. Nevertheless, as NHPs and humans have similar cellular distribution of TLRs [6], our results will guide future vaccine development. Another limitation of our NHP study is that we did not include soluble control group or other licensed vaccine formulations (e.g., lipid-based nanoparticles used in mRNA vaccination) due to limited resources. It would be interesting to directly compare their efficacies to sHDL-Ag + polyICLC in future NHP studies.

4. Conclusions.

We have examined immunogenicity of sHDL formulated with three different adjuvant systems, namely CpG ODNs (a TLR9 agonist, both type B and C) and polyICLC (a TLR3 agonist). Our results have shown that sHDL-Ag admixed with polyICLC promoted strong activation of DCs and significantly enhanced Ag-specific CD8+ T cell responses in mice, compared with free Ag + polyICLC group, which has been widely used in clinal trials [19, 40]. In addition, when combined with α-PD-1, sHDL-Ag + polyICLC vaccine formulation

exerted strong anti-tumor efficacy against established MC-38 tumors, leading to tumor eradication in 100% of treated animals. Excitingly, we have demonstrated that sHDL-Ag + polyICLC also induced robust Ag-specific, polyfunctional CD8+ T cell responses in NHPs, especially in combination with a viralvector vaccine. Overall, this work highlights the efficacy, versatility, and translational potential of the sHDL vaccine system for applications in vaccines and cancer immunotherapy.

Supplementary Material

Refer to Web version on PubMed Central for supplementary material.

Acknowledgements

This work was supported in part by NIH (R01EB022563, J.J.M.; R01CA210273, J.J.M.; R01AI127070, J.J.M; R01DK125087, J.J.M; R21NS091555, A.S.; R01HL134569, A.S.) J.J.M. is supported by NSF CAREER Award (1553831). E.B.O. was supported by NSERC Postdoctoral Fellowship and CIHR Postdoctoral Fellowship. D.A. is supported by Cancer Center Support Grant (P30 CA046592). We acknowledge the NIH Tetramer Core Facility (contract HHSN272201300006C) for the provision of MHC-I tetramers.

5. References.

[1]. Irvine DJ, Hanson MC, Rakhra K, Tokatlian T, Synthetic Nanoparticles for Vaccines and Immunotherapy, Chem Rev115 (2015) 11109–11146. [PubMed: 26154342]

[2]. Nam J, Son S, Park KS, Zou W, Shea LD, Moon JJ, Cancer nanomedicine for combination cancer immunotherapy, Nature Reviews Materials4 (2019) 398–414.

[3]. Yu C, An M, Li M, Liu H, Immunostimulatory properties of lipid modified CpG oligonucleotides, Molecular pharmaceutics14 (2017) 2815–2823. [PubMed: 28686452]

[4]. Bourquin C, Anz D, Zwiorek K, Lanz A-L, Fuchs S, Weigel S, Wurzenberger C, von der Borch P, Golic M, Moder S, Targeting CpG oligonucleotides to the lymph node by nanoparticles elicits efficient antitumoral immunity, The Journal of Immunology181 (2008) 2990–2998. [PubMed: 18713969]

[5]. Zorn GG, Khan S, Britten CM, Sommandas V, Camps MG, Loof NM, Budden CF, Meeuwenoord NJ, Filippov DV, van der Marel GA, Efficient induction of antitumor immunity by synthetic toll-like receptor ligand–peptide conjugates, Cancer immunology research2 (2014) 756–764. [PubMed: 24950688]

[6]. Thompson EA, Lore K, Non-human primates as a model for understanding the mechanism of action of toll-like receptor-based vaccine adjuvants, Curr Opin Immunol47 (2017) 1–7. [PubMed: 28715767]

[7]. Iwasaki A, Medzhitov R, Toll-like receptor control of the adaptive immune responses, Nature immunology5 (2004) 987. [PubMed: 15454922]

[8]. Speiser DE, Liénard D, Rufer N, Rubio-Godoy V, Rimoldi D, Lejeune F, Krieg AM, Cerottini J-C, Romero P, Rapid and strong human CD8+ T cell responses to vaccination with peptide, IFA, and CpG oligodeoxynucleotide 7909, Journal of Clinical Investigation115 (2005) 739.

[9]. Ballas ZK, Rasmussen WL, Krieg AM, Induction of NK activity in murine and human cells by CpG motifs in oligodeoxynucleotides and bacterial DNA, The Journal of Immunology157 (1996) 1840–1845. [PubMed: 8757300]

[10]. Hartmann G, Krieg AM, Mechanism and function of a newly identified CpG DNA motif in human primary B cells, The Journal of Immunology164 (2000) 944–953. [PubMed: 10623843]

[11]. Vollmer J, Weeratna R, Payette P, Jurk M, Schetter C, Laucht M, Wader T, Tluk S, Liu M, Davis HL, Characterization of three CpG oligodeoxynucleotide classes with distinct immunostimulatory activities, European journal of immunology34 (2004) 251–262. [PubMed: 14971051]

[12]. Valmori D, Souleimanian NE, Tosello V, Bhardwaj N, Adams S, O'Neill D, Pavlick A, Escalon JB, Cruz CM, Angiulli A, Vaccination with NY-ESO-1 protein and CpG in Montanide induces integrated antibody/Th1 responses and CD8 T cells through cross-priming, Proceedings of the National Academy of Sciences104 (2007) 8947–8952.

[13]. Karbach J, Gnjatic S, Bender A, Neumann A, Weidmann E, Yuan J, Ferrara CA, Hoffmann E, Old LJ, Altorki NK, Tumor-reactive CD8+ T-cell responses after vaccination with NY-ESO-1 peptide, CpG 7909 and Montanide® ISA-51: association with survival, International journal of cancer126 (2010) 909–918. [PubMed: 19728336]

[14]. Haining WN, Davies J, Kanzler H, Drury L, Brenn T, Evans J, Angelosanto J, Rivoli S, Russell K, George S, CpG oligodeoxynucleotides alter lymphocyte and dendritic cell trafficking in humans, Clinical cancer research14 (2008) 5626–5634. [PubMed: 18765557]

[15]. Speiser DE, Liénard D, Rufer N, Rubio-Godoy V, Rimoldi D, Lejeune F, Krieg AM, Cerottini J-C, Romero P, Rapid and strong human CD8+ T cell responses to vaccination with peptide, IFA, and CpG oligodeoxynucleotide 7909, The Journal of clinical investigation115 (2005) 739–746. [PubMed: 15696196]

[16]. Schulz O, Diebold SS, Chen M, Näslund T.l., Nolte MA, Alexopoulou L, Azuma Y-T, Flavell RA, Liljeström P, Sousa C.R. e, Toll-like receptor 3 promotes cross-priming to virus-infected cells, Nature433 (2005) 887–892. [PubMed: 15711573]

[17]. Kato H, Takeuchi O, Mikamo-Satoh E, Hirai R, Kawai T, Matsushita K, Hiiragi A, Dermody TS, Fujita T, Akira S, Length-dependent recognition of double-stranded ribonucleic acids by retinoic acid-inducible gene-I and melanoma differentiation-associated gene 5, J Exp Med205 (2008) 1601–1610. [PubMed: 18591409]

[18]. Matsumiya T, Stafforini DM, Function and regulation of retinoic acid-inducible gene-I, Critical Reviews™ in Immunology30 (2010).

[19]. Sultan H, Salazar AM, Celis E, Poly-ICLC, a multi-functional immune modulator for treating cancer, Semin Immunol49 (2020) 101414. [PubMed: 33011064]

[20]. Sultan H, Wu J, Fesenkova V.l., Fan AE, Addis D, Salazar AM, Celis E, Poly-IC enhances the effectiveness of cancer immunotherapy by promoting T cell tumor infiltration, J Immunother Cancer8 (2020).

[21]. Huang H, Cruz W, Chen J, Zheng G, Learning from biology: synthetic lipoproteins for drug delivery, Wiley Interdisciplinary Reviews: Nanomedicine and Nanobiotechnology7 (2015) 298–314. [PubMed: 25346461]

[22]. Kuai R, Ochyl LJ, Bahjat KS, Schwendeman A, Moon JJ, Designer vaccine nanodiscs for personalized cancer immunotherapy, Nature materials16 (2017) 489–496. [PubMed: 28024156]

[23]. Torre LA, Bray F, Siegel RL, Ferlay J, Lortet-Tieulent J, Jemal A, Global cancer statistics, 2012, CA: a cancer journal for clinicians65 (2015) 87–108. [PubMed: 25651787]

[24]. Yu C, An M, Li M, Liu H, Immunostimulatory Properties of Lipid Modified CpG Oligonucleotides, Mol Pharm14 (2017) 2815–2823. [PubMed: 28686452]

[25]. Wille-Reece U, Flynn BJ, Lore K, Koup RA, Miles AP, Saul A, Kedl RM, Mattapallil JJ, Weiss WR, Roederer M, Seder RA, Toll-like receptor agonists influence the magnitude and quality of memory T cell responses after prime-boost immunization in nonhuman primates, J Exp Med203 (2006) 1249–1258. [PubMed: 16636134]

[26]. Hassani Najafabadi A, Zhang J, Aikins ME, Najaf Abadi Z.l., Liao F, Qin Y, Okeke EB, Scheetz LM, Nam J, Xu Y, Adams D, Lester P, Hetrick T, Schwendeman A, Wicha MS, Chang AE, Li Q, Moon JJ, Cancer Immunotherapy via Targeting Cancer Stem Cells Using Vaccine Nanodiscs, Nano Lett20 (2020) 7783–7792. [PubMed: 32926633]

[27]. Scheetz L, Kadiyala P, Sun X, Son S, Hassani Najafabadi A, Aikins M, Lowenstein PR, Schwendeman A, Castro MG, Moon JJ, Synthetic High-density Lipoprotein Nanodiscs for Personalized Immunotherapy Against Gliomas, Clin Cancer Res26 (2020) 4369–4380. [PubMed: 32439701]

[28]. Kuai R, Sun X, Yuan W, Ochyl LJ, Xu Y, Najafabadi AH, Scheetz L, Yu M-Z, Balwani I, Schwendeman A, Dual TLR agonist nanodiscs as a strong adjuvant system for vaccines and immunotherapy, Journal of controlled release282 (2018) 131–139. [PubMed: 29702142]

[29]. Kuai R, Singh PB, Sun X, Xu C, Hassani Najafabadi A, Scheetz L, Yuan W, Xu Y, Hong H, Keskin DB, Robust Anti-Tumor T Cell Response with Efficient Intratumoral Infiltration by Nanodisc Cancer Immunotherapy, Advanced Therapeutics3 (2020) 2000094.

[30]. Xu C, Hong H, Lee Y, Park KS, Sun M, Wang T, Aikins ME, Xu Y, Moon JJ, Efficient Lymph Node-Targeted Delivery of Personalized Cancer Vaccines with Reactive Oxygen Species-Inducing Reduced Graphene Oxide Nanosheets, ACS Nano14 (2020) 13268–13278. [PubMed: 32902245]

[31]. Martinez-Murillo P, Tran K, Guenaga J, Lindgren G, Adori M, Feng Y, Phad GE, Vazquez Bernat N, Bale S, Ingale J, Dubrovskaya V, O'Dell S, Pramanik L, Spangberg M, Corcoran M, Lore K, Mascola JR, Wyatt RT, Karlsson Hedestam GB, Particulate Array of Well-Ordered HIV Clade C Env Trimers Elicits Neutralizing Antibodies that Display a Unique V2 Cap Approach, Immunity46 (2017) 804–817 e807. [PubMed: 28514687]

[32]. Kasturi SP, Rasheed MAU, Havenar-Daughton C, Pham M, Legere T, Sher ZJ, Kovalenkov Y, Gumber S, Huang JY, Gottardo R, Fulp W, Sato A, Sawant S, Stanfield-Oakley S, Yates N, LaBranche C, Alam SM, Tomaras G, Ferrari G, Montefiori D, Wrammert J, Villinger F, Tomai M, Vasilakos J, Fox CB, Reed SG, Haynes BF, Crotty S, Ahmed R, Pulendran B, 3M-052, a synthetic TLR-7/8 agonist, induces durable HIV-1 envelope-specific plasma cells and humoral immunity in nonhuman primates, Sci Immunol5 (2020).

[33]. Saunders KO, Pardi N, Parks R, Santra S, Mu Z, Sutherland L, Scearce R, Barr M, Eaton A, Hernandez G, Goodman D, Hogan MJ, Tombacz I, Gordon DN, Rountree RW, Wang Y, Lewis MG, Pierson TC, Barbosa C, Tam Y, Shen X, Ferrari G, Tomaras GD, Montefiori DC, Weissman D, Haynes BF, Lipid nanoparticle encapsulated nucleoside-modified mRNA vaccines elicit polyfunctional HIV-1 antibodies comparable to proteins in nonhuman primates, NPJ Vaccines6 (2021) 50. [PubMed: 33837212]

[34]. Park H, Adamson L, Ha T, Mullen K, Hagen S.l., Nogueron A, Sylwester AW, Axthelm MK, Legasse A, Piatak M Jr., Lifson JD, McElrath JM, Picker LJ, Seder RA, Polyinosinic-polycytidylic acid is the most effective TLR adjuvant for SIV Gag protein-induced T cell responses in nonhuman primates, J Immunol190 (2013) 4103–4115. [PubMed: 23509365]

[35]. Foulds KE, Donaldson M, Roederer M, OMIP-005: Quality and phenotype of antigen-responsive rhesus macaque T cells, Cytometry A81 (2012) 360–361. [PubMed: 22438313]

[36]. Kandimalla ER, Bhagat L, Yu D, Cong Y, Tang J, Agrawal S, Conjugation of ligands at the 5'-end of CpG DNA affects immunostimulatory activity, Bioconjug Chem13 (2002) 966–974. [PubMed: 12236778]

[37]. Yadav M, Jhunjhunwala S, Phung QT, Lupardus P, Tanguay J, Bumbaca S, Franci C, Cheung TK, Fritsche J, Weinschenk T, Modrusan Z, Mellman I, Lill JR, Delamarre L, Predicting immunogenic tumour mutations by combining mass spectrometry and exome sequencing, Nature515 (2014) 572–576. [PubMed: 25428506]

[38]. Casimiro DR, Wang F, Schleif WA, Liang X, Zhang ZQ, Tobery TW, Davies ME, McDermott AB, O'Connor DH, Fridman A, Bagchi A, Tussey LG, Bett AJ, Finnefrock AC, Fu TM, Tang A, Wilson KA, Chen M, Perry HC, Heidecker GJ, Freed DC, Carella A, Punt KS, Sykes KJ, Huang L, Ausensi VI, Bachinsky M, Sadasivan-Nair U, Watkins DI, Emini EA, Shiver JW, Attenuation of simian immunodeficiency virus SIVmac239 infection by prophylactic immunization with dna and recombinant adenoviral vaccine vectors expressing Gag, J Virol79 (2005) 15547–15555. [PubMed: 16306625]

[39]. Petitdemange C, Kasturi SP, Kozlowski PA, Nabi R, Quarnstrom CF, Reddy PBJ, Derdeyn CA, Spicer LM, Patel P, Legere T, Kovalenkov YO, Labranche CC, Villinger F, Tomai M, Vasilakos J, Haynes B, Kang CY, Gibbs JS, Yewdell JW, Barouch D, Wrammert J, Montefiori D, Hunter E, Amara RR, Masopust D, Pulendran B, Vaccine induction of antibodies and tissue-resident CD8+ T cells enhances protection against mucosal SHIV-infection in young macaques, JCI Insight4 (2019).

[40]. Sabbatini P, Tsuji T, Ferran L, Ritter E, Sedrak C, Tuballes K, Jungbluth AA, Ritter G, Aghajanian C, Bell-McGuinn K, Hensley ML, Konner J, Tew W, Spriggs DR, Hoffman EW, Venhaus R, Pan L, Salazar AM, Diefenbach CM, Old LJ, Gnjatic S, Phase I trial of overlapping long peptides from a tumor self-antigen and poly-ICLC shows rapid induction of integrated

immune response in ovarian cancer patients, Clin Cancer Res18 (2012) 6497–6508. [PubMed: 23032745]

[41]. Klinman DM, Xie H, Little SF, Currie D, Ivins BE, CpG oligonucleotides improve the protective immune response induced by the anthrax vaccination of rhesus macaques, Vaccine22 (2004) 2881–2886. [PubMed: 15246624]

[42]. McCluskie MJ, Pryde DC, Gervais DP, Stead DR, Zhang N, Benoit M, Robertson K, Kim IJ, Tharmanathan T, Merson JR, Davis HL, Enhancing immunogenicity of a 3'aminomethylnicotine-DT-conjugate anti-nicotine vaccine with CpG adjuvant in mice and non-human primates, Int Immunopharmacol16 (2013) 50–56. [PubMed: 23562759]

[43]. Shirota H, Klinman DM, Recent progress concerning CpG DNA and its use as a vaccine adjuvant, Expert Rev Vaccines13 (2014) 299–312. [PubMed: 24308579]

[44]. Speiser DE, Lienard D, Rufer N, Rubio-Godoy V, Rimoldi D, Lejeune F, Krieg AM, Cerottini JC, Romero P, Rapid and strong human CD8+ T cell responses to vaccination with peptide, IFA, and CpG oligodeoxynucleotide 7909, J Clin Invest115 (2005) 739–746. [PubMed: 15696196]

[45]. Kumar A, Dowling WE, Roman RG, Chaudhari A, Gurry C, Le TT, Tollefson S, Clark CE, Bernasconi V, Kristiansen PA, Status Report on COVID-19 Vaccines Development, Curr Infect Dis Rep23 (2021) 9. [PubMed: 33867863]

[46]. Ahi YS, Bangari DS, Mittal SK, Adenoviral vector immunity: its implications and circumvention strategies, Curr Gene Ther11 (2011) 307–320. [PubMed: 21453277]

Highlights

- Nano-vaccine elicits robust CD8+ T cell responses in mice and non-human primates.
- Nano-vaccine combined with anti-PD-1 IgG therapy exert robust anti-tumor efficacy.
- Nano-vaccine + polyICLC induce stronger T cell response than those with CpC-B or -C.

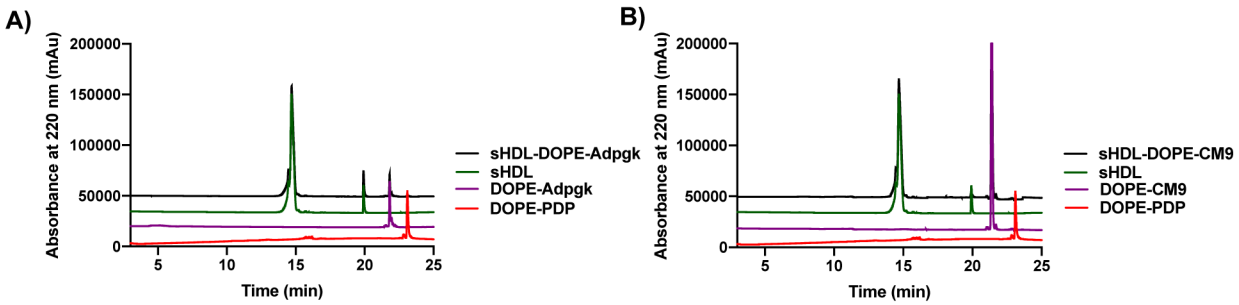

Figure 1. Characterization of sHDL loaded with Ag peptides.

Nanodiscs were analyzed by HPLC for quantification of Ag loading. **A-B)** Representative HPLC chromatograms are shown for **A)** sHDL-Adpgk and **B)** SHDL-CM9.

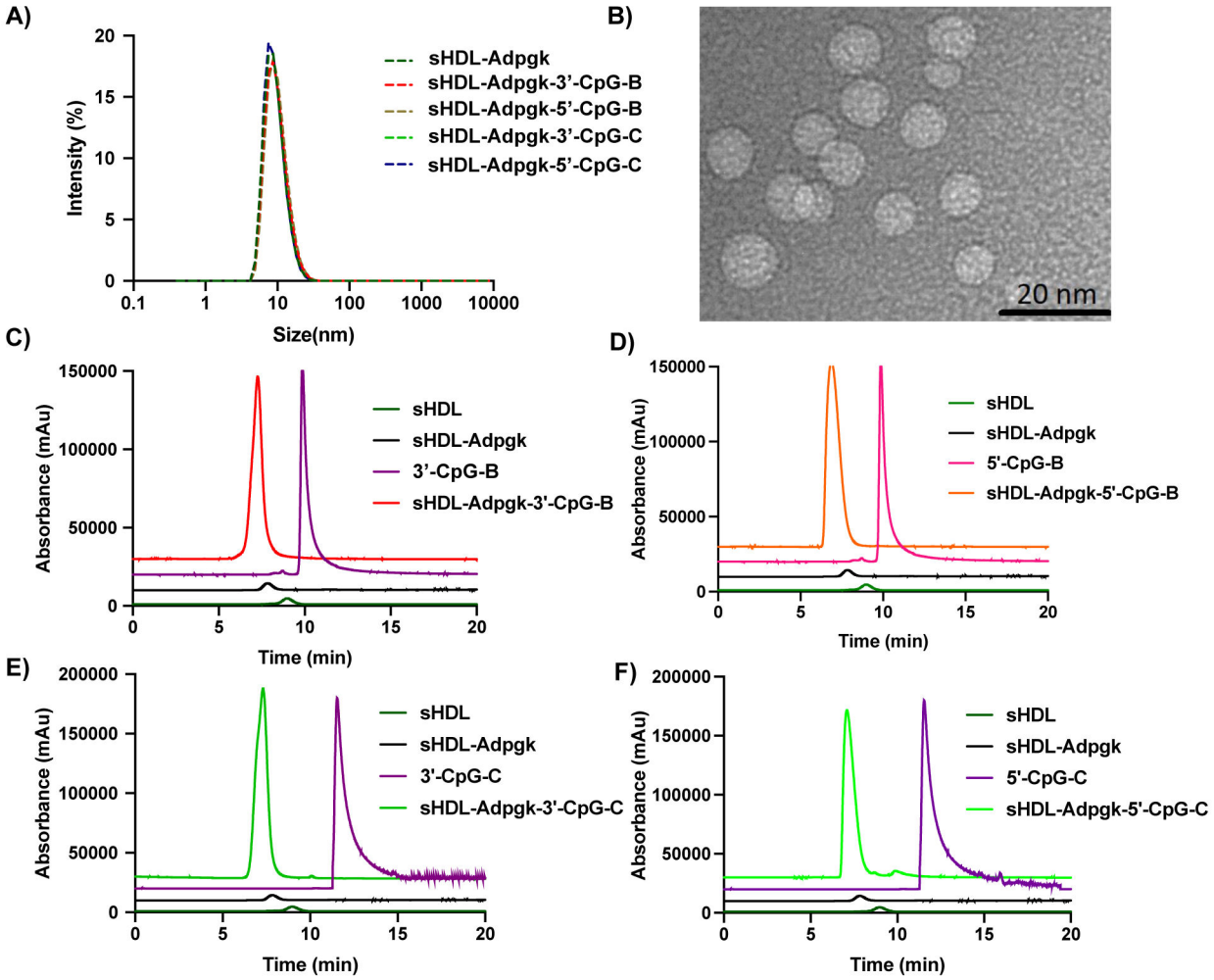

Figure 2. Characterization of sHDL-Adpgk-CpG.

A) Dynamic light scattering analysis of sHDL-Adpgk carrying CpG-B or CpG-C with cholesterol tethered at either 3' and 5' terminus. **B**) TEM image of sHDL-Adpgk-3'-CpG-C. **C-F)** GPC analyses of sHDL-Adpgk-CpG formulations, showing **C)** sHDL-Adpgk-3'-CpG-B, **D)** sHDL-Adpgk-5'-CpG-B, **E)** sHDL-Adpgk-3'-CpG-C, and **F)** sHDL-Adpgk-5'-CpG-C.

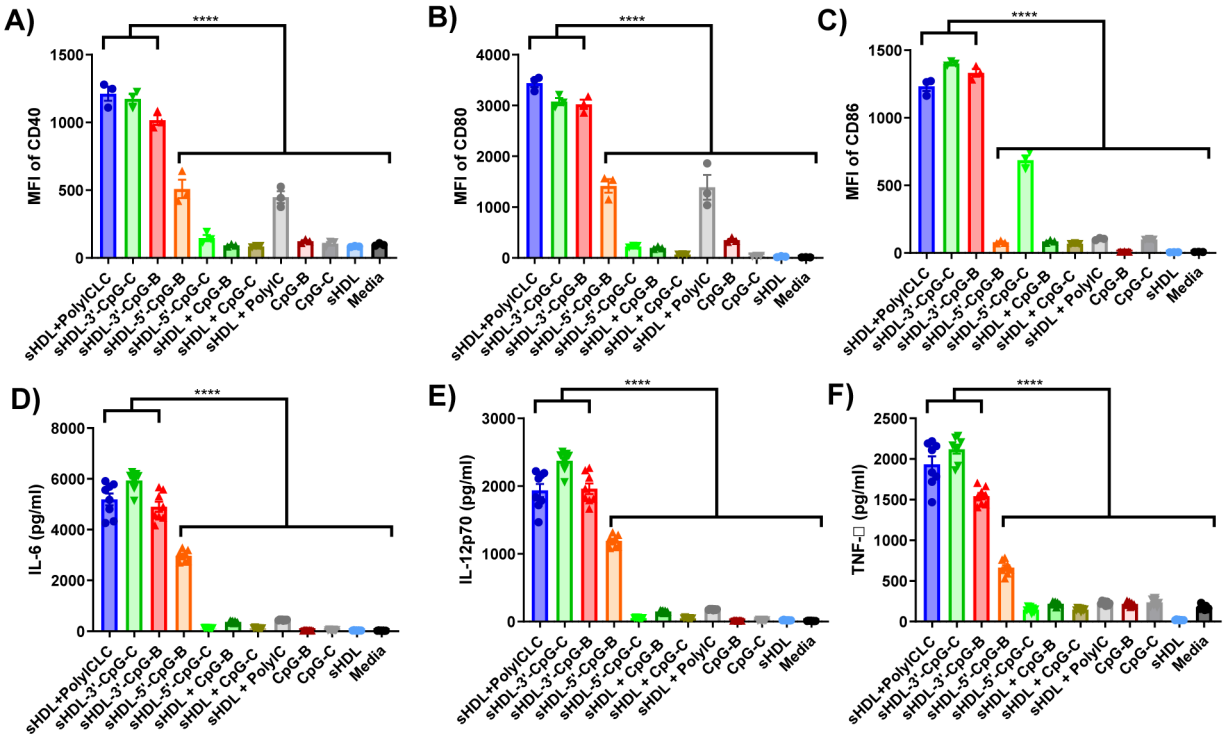

Figure 3. Stimulation of BMDCs with sHDL-adjuvant formulations.

BMDCs were incubated for 24 hours with various adjuvants in either soluble or sHDL formulations with 23 nM CpG or 20 μg polyICLC. The expression level of **A)** CD40, **B)** CD80, and **C)** CD86 on BMDCs were measured by flow cytometry. **D)** IL-6, **E)** IL-12p70, and **F)** TNF-α secreted by BMDCs were measured by ELISA. Data show the mean ± SEM (n = 8). Statistical significance was calculated by one-way ANOVA, followed by the Tukey's multiple comparisons post-test. ****P < 0.0001.

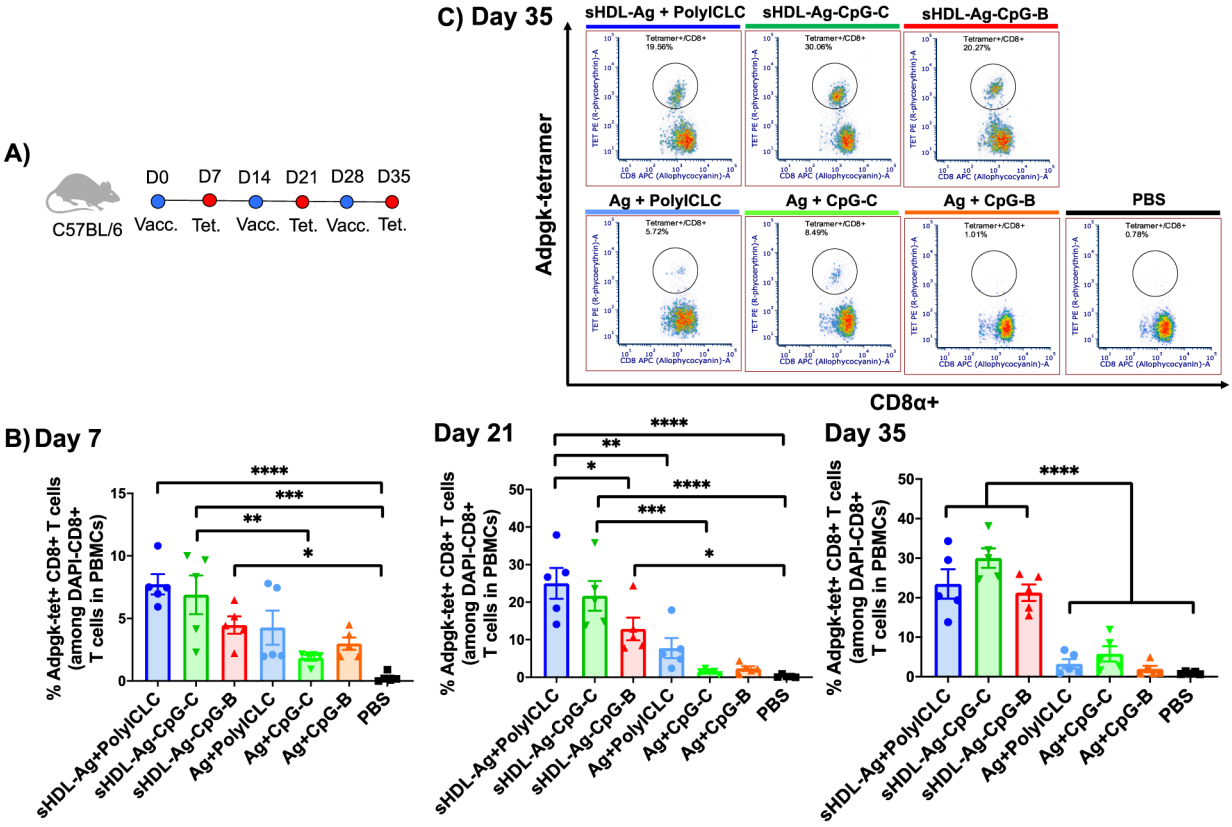

Figure 4. sHDL vaccine nanodiscs elicit strong antigen-specific CD8+ T cell responses.

A) C57BL/6 mice were immunized with nanodisc formulations (15.5 nmol Adpgk peptide, 2.3 nmol CpG, or 60 μg polyICLC) on days 0, 14, and 28. **B)** On days 7, 21, and 35, the frequency of Adpgk-specific CD8α+ T cells among PBMCs was measured. **C)** Shown are representative scatter plots for Adpgk-specific CD8α+ T cells on day 35. Data represent mean ± SEM, n = 5. Statistical significance was calculated by one-way ANOVA, followed by the Tukey's multiple comparisons post-test. *P < 0.05, **P < 0.01, ***P < 0.001, and ****P < 0.0001.

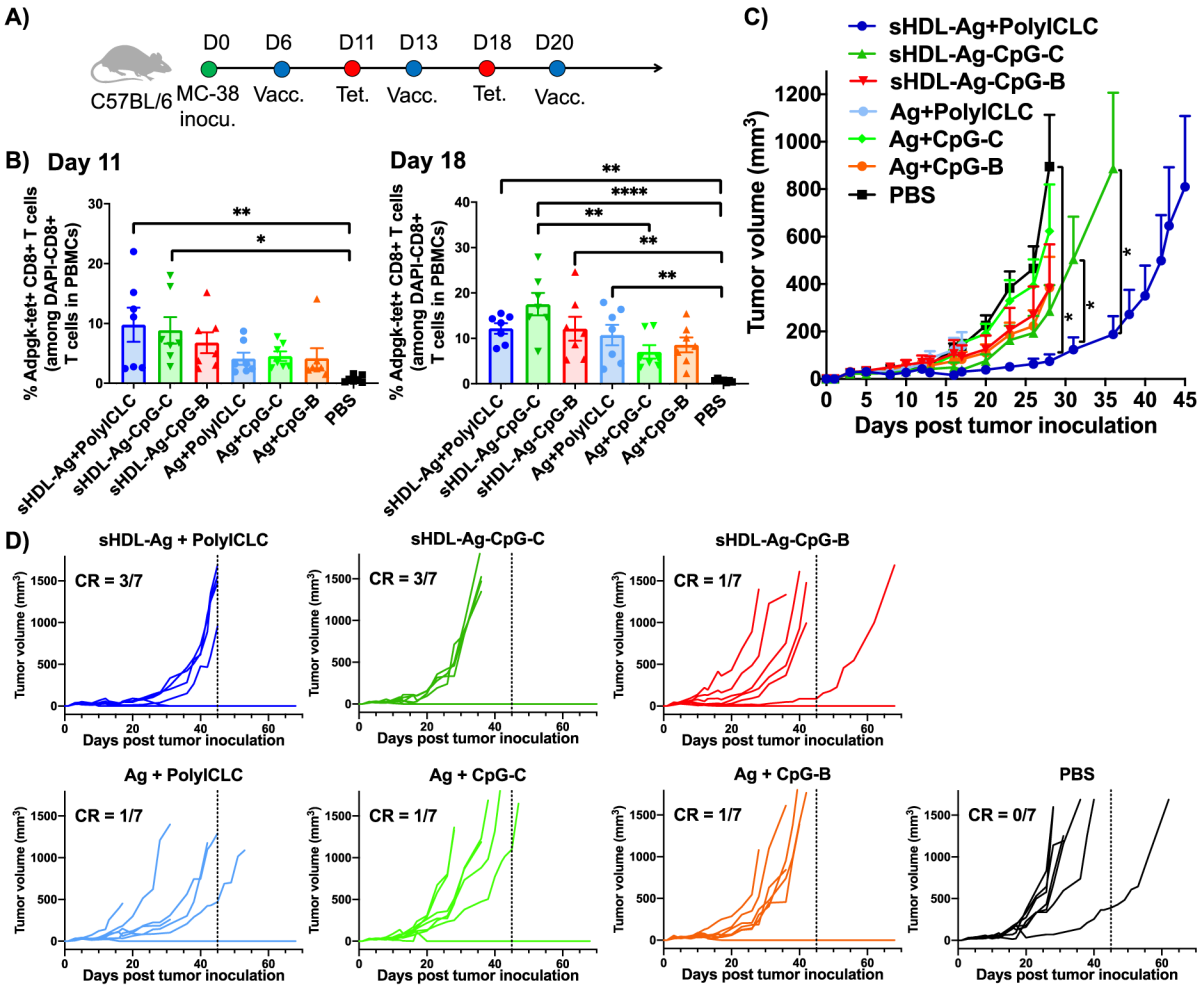

Figure 5. sHDL nanodiscs for vaccination against tumor-specific neoantigen.

A) C57BL/6 mice were inoculated subcutaneously with $1x10^6$ MC-38 tumor cells and immunized with various vaccine formulations (15.5 nmol Ag peptide, 2.3 nmol CpG, or 60 μg polyICLC) on days 6, 13, and 20. **B)** Shown are the percentages of Adpgk-specific CD8α+ T cells among PBMCs on days 11 and 18. Shown are the **C)** average and **D)** individual tumor growth. Data represent mean ± SEM, n = 7. Statistical significance was calculated by B) one-way ANOVA, or C) two-away ANOVA, followed by the Tukey's multiple comparisons post-test. *P < 0.05, **P< 0.01, and ****P < 0.0001.

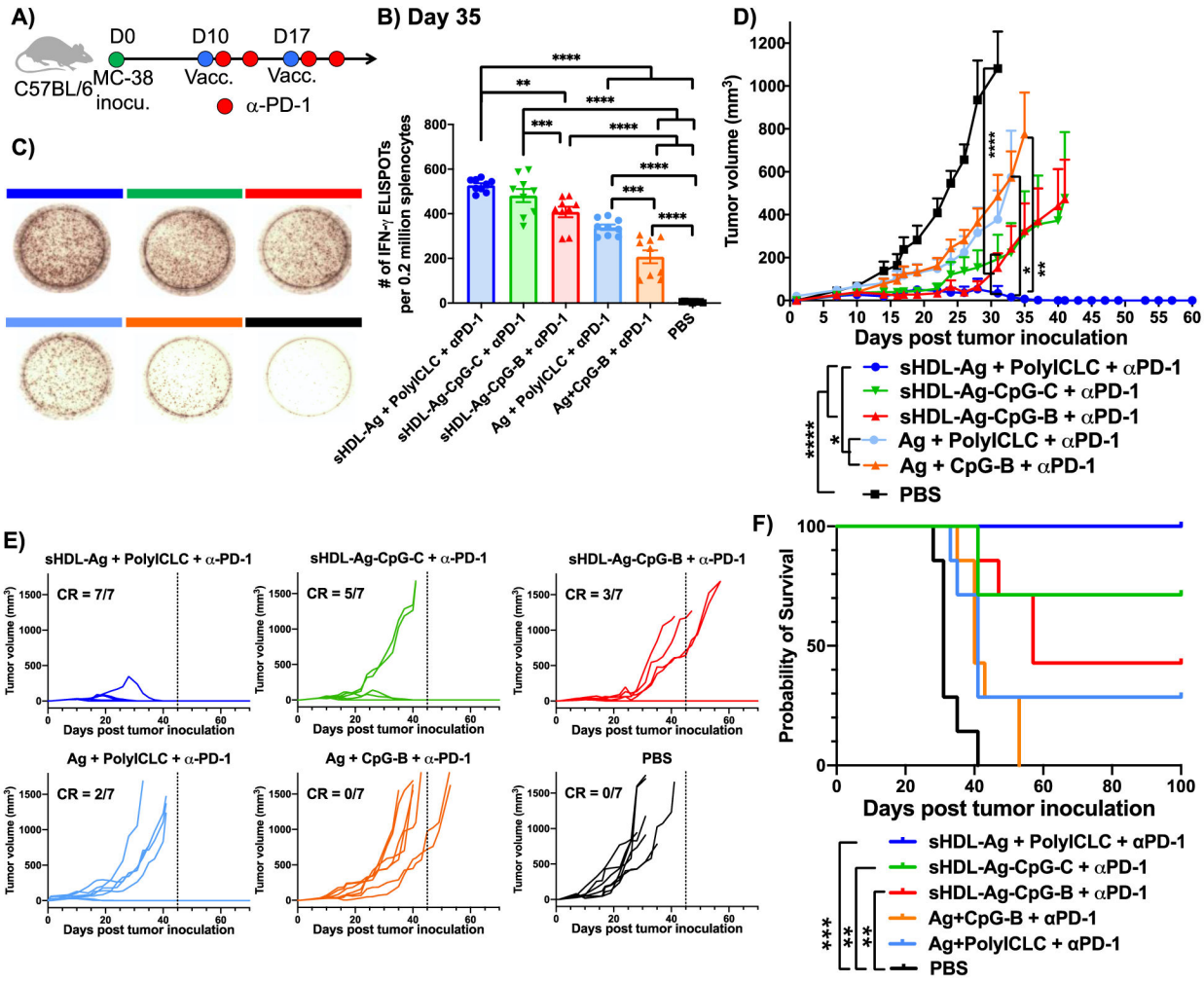

Figure 6. sHDL nanodiscs for vaccination against mutated tumor-specific neoantigen.

A) C57BL/6 mice were inoculated subcutaneously with $1x10^6$ MC-38 tumor cells and immunized with various vaccine formulations (15.5 nmol Ag peptide, 2.3 nmol CpG, or 60 μg polyICLC) on days 10 and 17. In addition, 100 μg α-PD-1 IgG was administered on days 1 and 4 after each vaccination. **B)** IFN-γ ELISPOT assay was performed on day 35 after *ex vivo* restimulation of splenocytes with 10 μg/mL Adpgk peptide, and **C)** representative ELISPOT wells are shown. **D-F)** Vaccinated mice were monitored for **D,E)** the tumor growth and **F)** survival. Data represent mean ± SEM, n = 7. Statistical significance was calculated by **B)** one-way ANOVA or **E)** two-away ANOVA, followed by the Tukey's multiple comparisons post-test, or **F)** by Kaplan-Meier survival analysis with Log-rank Mantel-Cox. *P < 0.05, **P< 0.01, ***P < 0.001, and ****P < 0.0001.

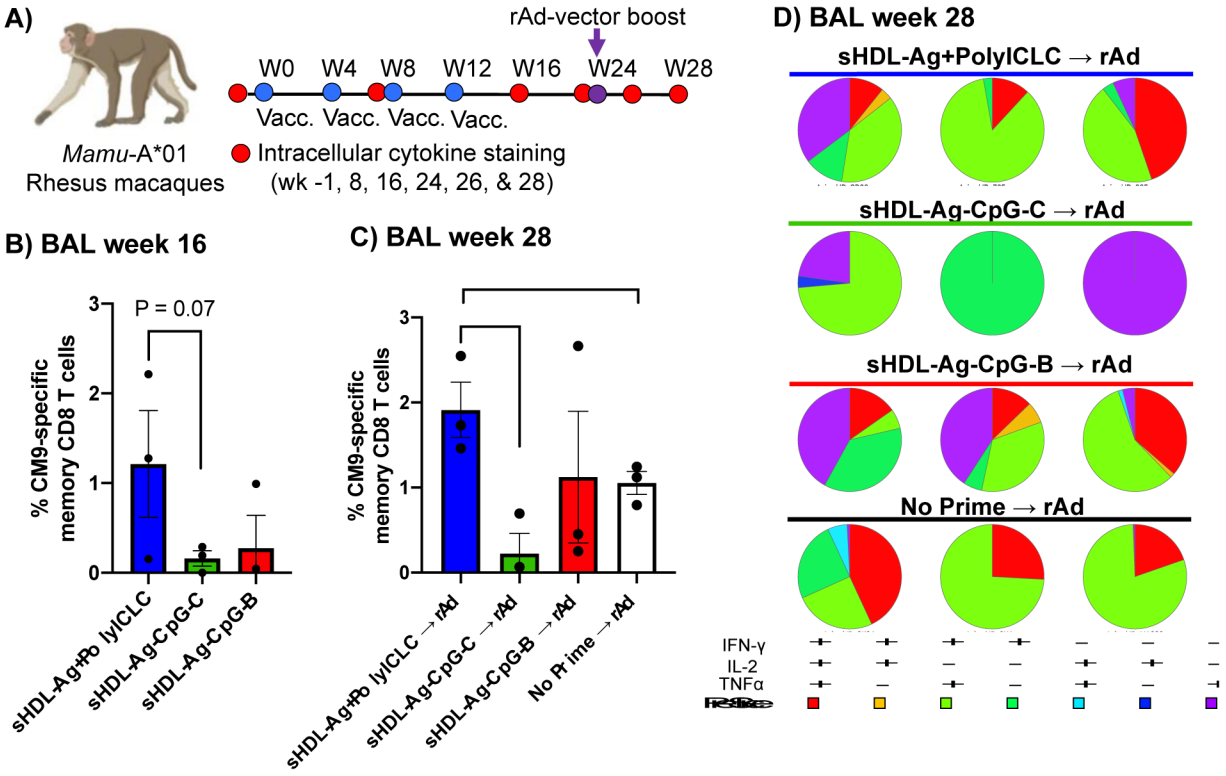

Figure 7. sHDL vaccination elicits robust T cell responses in NHPs.

A) *Mamu*-A*01 rhesus macaques were immunized subcutaneously on weeks 0, 4, 8, and 12 with SIV Gag CM9 epitope formulated in sHDL with polyICLC, CpG-2395 (CpG-C), or CpG-7909 (CpG-B). After resting for 10 weeks, macaques were boosted via intramuscular administration of rAd5 vector encoding SIVmac239-Gag (rAd). **B-D)** Memory CD8+ T cell responses specific to Gag CM9 in BAL tissues were measured by intracellular cytokine staining. Shown are the data for **B)** week 16 (4 weeks after the 4th sHDL vaccination) and on **C)** week 28 (4 weeks after the rAd boost). **D)** Quality of the CD8+ T cell response after rAd5 vector boost is shown for BAL tissues on week 28. CD8+ T cell cytokine responses were divided into seven distinct subpopulations producing any combination of IFN-γ, IL2, and TNF-α. Data represent mean ± SEM, n = 3. *P < 0.05, **P< 0.01.

Table 1.

Characterization of sHDL-Adpgk-CpG formulations.

	Cho-CpG incorporated in sHDL-Adpgk	Hydrodynamic Size (nm)
Cholesterol-3'-CpG-C (2395)	90 ± 2%	10 ± 6
Cholesterol-5'-CpG-C (2395)	88 ± 4%	12 ± 3
Cholesterol-3'-CpG-B (1826)	90 ± 6%	10 ± 7
Cholesterol-5'-CpG-B (1826)	90 ± 7%	11 ± 7